Romanian Reports in Physics, Vol. 67, No. 3, P. 872–889, 2015

VALUES OF THE PHASE SPACE FACTORS INVOLVED IN DOUBLE BETA DECAY

MIHAIL MIREA[1,2], TUDOR PAHOMI[2,3], SABIN STOICA[1,2]

[1]Horia Hulubei Foundation, P.O. MG12, 077125-Magurele, Romania
[2]Horia Hulubei National Institute of Physics and Nuclear Engineering, P.O. Box MG6, 077125-Magurele, Romania
[3]University of Bucharest, Faculty of Physics, P.O. Box MG11, 077125-Magurele, Romania

Received April 27, 2015

Abstract. We report an up-dated and complete list of the phase space factors (PSF) for the $\beta^-\beta^-$, $\beta^+\beta^+$, $EC\beta^+$ and $ECEC$ double beta decay (DBD) modes. In calculation, the Coulomb distortion of the electron wave functions is treated by solving numerically the Dirac equation with inclusion of the finite nuclear size and electron screening effects. In addition to the previous recent calculations we used a Coulomb potential derived from a realistic proton density distribution in nucleus, developed own routines with improved precision for solving the Dirac equations and integrating the PSF expressions, and used $Q^{\beta\beta}$-values reported recently. In general, we found a good agreement between our PSF values and those reported by other authors, especially for $\beta^-\beta^-$ and $\beta^+\beta^+$ decay modes and lighter nuclei. However, even in these cases we got several relevant discrepancies (larger than 10%) between our results and those reported in literature, while for the EC decay modes we got more and larger discrepancies. The possible sources of these discrepancies are discussed. Accurate values of the PSF are necessary ingredients both for theorists, to improve the DBD lifetime predictions and constraint the neutrino parameters, and for experimentalists to plan their set-ups.

Key words: Double beta decay, phase space factors, electron wave functions.

1. INTRODUCTION

Double beta decay is the most rare nuclear process measured so far, which presents a great interest especially for testing the lepton number conservation (LNC) and understanding the neutrino properties. Within the Standard Model (SM) it can occur through several decay modes that conserve the lepton number, with the emission of two neutrinos/anti-neutrinos (2ν). However, theories beyond SM predict that this process may also occur without LNC, and hence without emission of neutrinos/anti-neutrinos, through the so called neutrinoless (0ν) decay modes. According to the number and type of the released leptons, we may have the following DBD modes: i) two neutrino double-electron decay ($2\nu\beta^-\beta^-$); ii) neutrinoless double-electron decay ($0\nu\beta^-\beta^-$); iii) two neutrino double-positron decay ($2\nu\beta^+\beta^+$); iv) neutrinoless double-positron decay ($0\nu\beta^+\beta^+$); v) two neutrino electron capture positron emitting decay ($2\nu EC\beta^+$); vi) neutrinoless electron capture positron emitting de-

cay ($0\nu EC\beta^+$); vii) two neutrino double electron capture decay ($2\nu ECEC$) and viii) neutrinoless double electron capture decay ($0\nu ECEC$). Complete information about the achievements in the study of DBD can be found in several excellent recent reviews [1–4], which, in turn, contain a comprehensive list of references in domain. The lifetimes for the DBD modes can be written as follows [5, 6] :

$$\left(T_{1/2}^{2\nu}\right)^{-1} = G_{2\nu}^{m}(E_0, Z) g_A^4 \mid m_e c^2 M_{2\nu} \mid^2 \qquad (1)$$
$$\left(T_{1/2}^{0\nu}\right)^{-1} = G_{0\nu}^{m}(E_0, Z) g_A^4 \mid M_{0\nu} \mid^2 \left(< m_\nu > /m_e\right)^2 \ ,$$

where $G_{2\nu,0\nu}$ and $M_{2\nu,0\nu}$ are the phase space factors and matrix elements for the 2ν and 0ν decay modes, m_e and m_ν are the electron and neutrino masses, g_A is the axial vector coupling constant and m denotes one the DBD modes i)-vii). For the 0ν decay mode we consider here only the light neutrino exchange mechanism.

The purpose of this work is to give an up-dated and complete list of the PSF values for the i)-vii) DBD modes mentioned above for transitions to final ground states (g.s.) and to (possible) excited 2_1^+ and 0_1^+ states. The decay mode $0\nu ECEC$ can not occur to the order of approximation that is presently considered in literature. We developed new routines to compute the relativistic (Dirac) electron w.f., with the inclusion of nuclear finite size and screening effects. In addition to the previous recent calculations, we use a Coulomb potential derived from a realistic proton density distribution in nucleus, develop own routines with improved precision for solving the Dirac equations and integrating the PSF expressions, and take $Q^{\beta\beta}$ values from a recent work [7]. Also, we report for the first time PSF values for transitions to final excited 2_1^+ states computed with exact Dirac electron functions. In general, we found a good agreement between our PSF values and those reported by other authors, especially for $\beta^-\beta^-$ and $\beta^+\beta^+$ decay modes and lighter nuclei. However, even in these cases we got several relevant discrepancies (larger than 10%) between our results and those reported in literature, while for the EC decay modes we got more and larger discrepancies. The possible sources of these discrepancies are discussed. Accurate PSF values (besides the NME [8–24]) are necessary ingredients both for theorists to improve the DBD lifetime predictions and constraint the neutrino parameters, and for experimentalists to plan their set-ups.

2. THEORETICAL FRAMEWORK

To compute PSF for DBD decay modes we need first to obtain the w.f. of the electron(s)/positron(s) emitted or electron(s) captured in the decay, which are distorted by the Coulomb potential of the nucleus. Older calculations have used a non-relativistic approach where the distortion of the w.f. by the Coulomb field was

considered through Fermi (Coulomb) factors obtained (for the emitted particles) by taking the square of the ratio of the Schrödinger scattering solution for a point charge Z to a plane wave, evaluated at the origin [25, 26]. In a better approximation, the Fermi factors are calculated using a relativistic treatment of the electron/positron w.f, but with approximate Dirac functions (the Fermi factor is defined as the square of the ratio of the values of the Dirac w.f. of the electron at the nuclear surface) and without inclusion of screening effects [27–32]. Recently, Kotila and Iachello (KI) recalculated the PSF using exact Dirac electron/positron w.f. and including the screening effect [5, 6]. To obtain the radial electron/positron w.f. they solved the Dirac equation using the subroutines package RADIAL [38]. In this work we adopt this more rigorous relativistic treatment but building up own routines and including additional ingredients, as it is described in the following.

2.1. THE RADIAL WAVE FUNCTIONS

For free states we use relativistic scattering electron/positron w.f., solutions of the Dirac equation in a central (Coulomb) potential:

$$\Psi^{+}_{\epsilon\kappa\mu}(r) = \begin{pmatrix} g_\kappa(\epsilon,r)\chi^{\mu}_{\kappa} \\ if_\kappa(\epsilon,r)\chi^{\mu}_{-\kappa} \end{pmatrix} \tag{2}$$

for β^- decay and

$$\Psi^{-}_{\epsilon\kappa\mu} = \begin{pmatrix} if_\kappa(\epsilon,r)\chi^{-\mu}_{-\kappa} \\ -g_\kappa(\epsilon,r)\chi^{-\mu}_{\kappa} \end{pmatrix} \tag{3}$$

for β^+ decay where $\kappa = (l-j)(2j+1)$ is the relativistic quantum number and χ^{μ}_{κ} are spherical spinors. The quantities $g_\kappa(\epsilon,r)$ and $f_\kappa(\epsilon,r)$ are the large and small components of the radial w.f. which satisfy the radial equations:

$$\begin{aligned} \frac{dg_\kappa(\epsilon,r)}{dr} &= -\frac{\kappa}{r}g_\kappa(\epsilon,r) + \frac{\epsilon - V + m_e c^2}{c\hbar}f_\kappa(\epsilon,r) \\ \frac{df_\kappa(\epsilon,r)}{dr} &= -\frac{\epsilon - V - m_e c^2}{c\hbar}g_\kappa(\epsilon,r) + \frac{\kappa}{r}f_\kappa(\epsilon,r) \end{aligned} \tag{4}$$

where V can be negative/positive (for β^-/β^+). These functions are normalized so that they have the following asymptotic behavior:

$$\begin{pmatrix} g_k(\epsilon,r) \\ f_k(\epsilon,r) \end{pmatrix} \sim \frac{\hbar e^{-i\delta_k}}{pr} \begin{pmatrix} \sqrt{\frac{\epsilon+m_e c^2}{2\epsilon}}\sin(kr - l\frac{\pi}{2} - \eta\ln(2kr) + \delta_k) \\ \sqrt{\frac{\epsilon-m_e c^2}{2\epsilon}}\cos(kr - l\frac{\pi}{2} - \eta\ln(2kr) + \delta_k) \end{pmatrix} \tag{5}$$

Here c is the speed of the light, m_e/ϵ are the electron mass/energy, $k = p/\hbar$ is the electron wave number, $\eta = Ze^2/\hbar v$ (with $Z = \pm Z$ for $\beta^{\mp}$ decays), is the Sommerfeld parameter, δ_κ is the phase shift and V is the Coulomb interaction energy between the

electron and the daughter nucleus. For the continuum spectrum, the radial function is normalized to the asymptotic form of the Coulomb function. The phase shifts are obtained by matching the inner numerical solution to the analytic function.

The bound states w.f. for the electron

$$\Psi^b_{\epsilon_n\kappa\mu}(r) = \begin{pmatrix} g^b_{n,\kappa}(r)\chi^\mu_\kappa \\ if^b_{n,\kappa}(r)\chi^\mu_{-\kappa} \end{pmatrix} \tag{6}$$

are solutions of the Dirac equation (4) and correspond to the eigenvalues ϵ_n (n is the radial quantum number). The quantum number κ is related to the total angular momentum $j_\kappa = \mid \kappa \mid -1/2$. For simplicity, the quantities $g_{n,\kappa}(r) = rg^b_{n,\kappa}(r)$ and $f_{n,\kappa}(r) = rf^b_{n,\kappa}(r)$ are used in the following. These wave functions are normalized such that

$$\int_0^\infty [g^2_{n,\kappa}(r) + f^2_{n,\kappa}(r)]dr = 1. \tag{7}$$

An asymptotic solution is obtained by means of the WKB approximation and by considering that the potential V is negligible small:

$$\frac{f_{n,\kappa}}{g_{n,\kappa}} = \frac{c\hbar}{\epsilon + m_e c^2}\left(\frac{g'_{n,\kappa}}{g_{n,\kappa}} + \frac{\kappa}{r}\right) \tag{8}$$

where

$$\frac{g'_{n,\kappa}}{g_{n,\kappa}} = -\frac{1}{2}\mu'\mu^{-1} - \mu \tag{9}$$

with

$$\mu = \left[\frac{\epsilon + m_e c^2}{\hbar^2 c^2}(V - \epsilon + m_e c^2) + \frac{\kappa^2}{r^2}\right]^{1/2}. \tag{10}$$

In our calculations we use n=0 and n=1 number of nodes, for the orbitals $1s_{1/2}$ and $2s_{1/2}$, κ being -1. The eigenvalues of the discrete spectrum are obtained by matching two numerical solutions of the Dirac equation: the inverse solution that starts from the asymptotic conditions and the direct one that starts at r=0.

2.2. THE COULOMB POTENTIAL

The nuclear size corrections are usually taken into account by considering an unscreened potential V obtained for a uniform charge distribution in a sphere of radius R_A [27], [5]:

$$V(Z,r) = \begin{cases} -\frac{Z\alpha\hbar c}{r}, & r \geq R_A, \\ -Z(\alpha\hbar c)\left(\frac{3-(r/R_A)^2}{2R_A}\right), & r < R_A, \end{cases} \tag{11}$$

where generalized atomic units are used. The values of $\hbar$, of the electron charge e and its mass m_e are considered as unity. The energy unit is $E_0 = me^4/h^4 = 27.2114$

eV, the Bohr radius is $a_0 = \hbar^2/m_e e^2$=0.529177 and the speed of the light in vacuum is c=137.036 (the inverse of the fine structure constant).

In this work we take into account the influence of the nuclear structure by using a potential $V(r)$ derived from a realistic proton density distribution in the nucleus. This is done by solving the Schrödinger equation for a Woods-Saxon potential. In this case:

$$V(Z,r) = \alpha\hbar c \int \frac{\rho_e(\vec{r'})}{\mid \vec{r} - \vec{r'} \mid} d\vec{r'} \tag{12}$$

where the charge density is

$$\rho_e(\vec{r}) = \sum_i (2j_i + 1) v_i^2 \mid \Psi_i(\vec{r}) \mid^2 \tag{13}$$

Ψ_i is the proton (Woods-Saxon) w. f. of the spherical single particle state i and v_i is its occupation amplitude. The factor $(2j_i + 1)$ reflects the spin degeneracy.

As an example, the difference between the behavior of the constant charge density ρ_e and the realistic charge density is displayed in Fig. 1 for the daughter nucleus ^{150}Sm. We computed the Coulomb potential with formula (12). In this case, the differences given by the charge densities are translated in a shift of 0.5 MeV energy in the potential at $r = 0$. This difference in energy vanishes when r increases, but is able to affect the values of the w.f.

The screening effect is taken into account by multiplying the expression of $V(r)$ with a function $\phi(r)$, which is the solution of the Thomas Fermi equation: $d^2\phi/dx^2 = \phi^{3/2}/\sqrt{x}$, with $x = r/b$, $b \approx 0.8853 a_0 Z^{-1/3}$ and a_0 = Bohr radius. It is calculated within the Majorana method [33]. The boundary conditions are $\phi(0) = 1$ and $\phi(\infty) = 0$. The screening effect is taken into account in the same manner as in Ref. [5]. The modality in which the screening function modifies the Coulomb potential depends on the specific mechanism and its boundary conditions.

In the case of the $\beta^-\beta^-$ process, the potential used to obtain the electron w.f. is:

$$rV_{\beta^-\beta^-}(Z,r) = (rV(Z,r) + 2) \times \phi(r) - 2 \tag{14}$$

to take into account the fact that DBD releases a final positive ion with charge +2. $V(Z,r)$ is negative. In our approach, we considered the solution of the Thomas-Fermi equation as an universal function, giving an effective screening. Here, the product $\alpha\hbar c$=1, for atomic units. The asymptotic potential between an electron and a double ionized atom is $rV_{\beta^-\beta^-} = -2$. In this case, the charge number $Z = Z_0 + 2$ corresponds to the daughter nucleus, Z_0 being the charge number of the parent nucleus. In the case of the $\beta^+\beta^+$ process, the potential used to obtain the electron wave functions is:

$$rV_{\beta^+\beta^+}(Z,r) = (rV(Z,r) + 2) \times \phi(r) - 2 \tag{15}$$

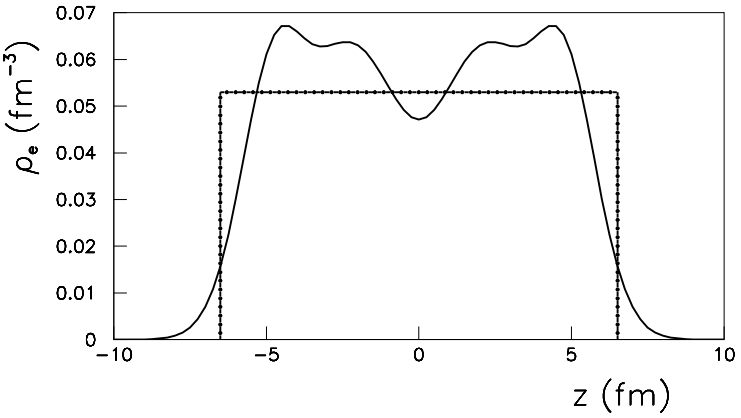

Fig. 1 – Profile of the realistic proton density ρ_e for ^{150}Sm (thick line) compared with that given with the constant density approximation (dot-dashed line).

where the final configuration is characterized by an ion with charge -2. $V(Z,r)$ is positive. In this case, the daughter nucleus has the charge number $Z = Z_0 - 2$. In both approaches, at r=0 the potential is unscreened because $\phi(0)$=1. Asymptotically $\phi(r)$ tends to 0 and we are left with the charge number of the final system.

In the case of the EC process, the potential used to obtain the electron w.f. reads:

$$rV_{EC}(Z,r) = (rV(Z,r)+1) \times \phi(r) - 1 \tag{16}$$

and the charge number $Z = Z_0$ corresponds to the parent nucleus. $V(Z,r)$ is negative. In the case of the β^+ process, the potential used to obtain the positron wave functions reads:

$$rV_{\beta^+}(Z,r) = (rV(Z,r)+1) \times \phi(r) - 1 \tag{17}$$

to take into account that in the final configuration we have an ion with charge -1. $V(Z,r)$ is positive. In this case the daughter nucleus has the charge number $Z = Z_0 - 1$. In the case of the $ECEC$ process, the potential used to obtain the electron w. f. is:

$$V_{ECEC}(Z,r) = V(Z,r) \times \phi(r) \tag{18}$$

and $Z = Z_0$, the final system being neutral.

2.3. CALCULATION OF THE PHASE SPACE FACTORS

2.3.1. Double Electron and Double Positron decay modes

To compute the PSF, we have to obtain the electron phase factors $f_{jk}^{(0)}$

$$f_{11}^{(0)} = \mid f^{-1-1} \mid^2 + \mid f_{11} \mid^2 + \mid f^{-1}_{\ 1} \mid^2 + \mid f_1^{\ -1} \mid^2 \tag{19}$$

with

$$f^{-1-1} = g_{-1}(\epsilon_1)g_{-1}(\epsilon_2)\ ;\ f_{11} = f_1(\epsilon_1)f_1(\epsilon_2), \tag{20}$$

$$f^{-1}{}_1 = g_{-1}(\epsilon_1)f_1(\epsilon_2)\ ;\ f_1{}^{-1} = f_1(\epsilon_1)g_1(\epsilon_2) \tag{21}$$

from the solutions of the Dirac equation by considering s-wave states and neglecting the neutrino mass. The values of the f and g functions are approximated with the solutions at the nuclear surface (the method I from [5]).

$$g_{-1}(\epsilon) = g_{-1}(\epsilon, R_A)\ ;\ f_1(\epsilon) = f_1(\epsilon, R_A) \tag{22}$$

where $R_A = 1.2A^{1/3}$ fm is the nuclear radius. For the $2\nu\beta\beta$ decay mode and transitions to g.s., the PSF expression reads:

$$\begin{aligned} G_{2\nu}^{\beta\beta}(0^+ \to 0^+) = \frac{2\tilde{A}^2}{3\ln 2 g_A^4 (m_e c^2)^2} \int_{m_e c^2}^{Q^{\beta\beta}+m_e c^2} d\epsilon_1 \\ \times \int_{m_e c^2}^{Q^{\beta\beta}+2m_e c^2-\epsilon_1} d\epsilon_2 \int_0^{Q^{\beta\beta}+2mc_e^2-\epsilon_1-\epsilon_2} d\omega_1 \\ \times f_{11}^{(0)} w_{2\nu}(\langle K_N\rangle^2 + \langle L_N\rangle^2 + \langle K_N\rangle\langle L_N\rangle) \end{aligned} \tag{23}$$

where $Q^{\beta\beta} = M(A, Z_0) - M(A, Z_0 - 2) - 4m_e c^2$ is the kinetic energy released in the process. $\langle K_N\rangle$, $\langle L_N\rangle$ are expressions that depend on the electron/positron ($\epsilon_{1,2}$) and neutrino ($\omega_{1,2}$) energies, and on the g.s. energy of the parent nucleus and on the excited states energy of the intermediate nucleus [26].

$$\langle K_N\rangle = \frac{1}{\epsilon_1 + \omega_1 + \langle E_N\rangle - E_I} + \frac{1}{\epsilon_2 + \omega_2 + \langle E_N\rangle - E_I} \tag{24}$$

$$\langle L_N\rangle = \frac{1}{\epsilon_1 + \omega_2 + \langle E_N\rangle - E_I} + \frac{1}{\epsilon_2 + \omega_1 + \langle E_N\rangle - E_I} \tag{25}$$

Here, the difference in energy in the denominator can be obtained from the approximation $\tilde{A}^2 = [W_0/2 + \langle E_N\rangle - E_I]^2$, where $\tilde{A} = 1.12A^{1/2}$ (in MeV) gives the energy of the giant Gamow-Teller resonance in the intermediate nucleus. The quantity W_0 is related to the Q value of the process and

$$w_{2\nu} = \frac{g_A^4 (G\cos\theta_C)^4}{64\pi^7\hbar} \omega_1^2 \omega_2^2 (p_1 c)(p_2 c)\epsilon_1\epsilon_2, \tag{26}$$

where ω_1 and $\omega_2 = Q^{\beta\beta} - \epsilon_1 - \epsilon_2 - \omega_1 + 2m_e c^2$ are the neutrino energies. The PSF are finally renormalized to the electron rest energy and are reported in $[yr^{-1}]$.

The PSF for the $2\nu\beta\beta$ decay mode and transitions to excited 0_1^+ states is calculated with a formula similar to (23), but replacing $Q^{\beta\beta}$ by $Q(0_1^+) = Q^{\beta\beta} - E_x(0_1^+)$, which is the kinetic energy released in this transition. $E_x(0_1^+)$ is the energy of the excited 0_1^+ state of the daughter nucleus x.

For the $2\nu\beta\beta$ decay mode and transitions to excited 2_1^+ states, the PSF formula reads [5, 6, 32, 34, 35]:

$$G_{2\nu}^{\beta\beta}(0^+ \to 2_1^+) = \frac{2\tilde{A}^6}{\ln 2 g_A^4 (m_e c^2)^6} \int_{m_e c^2}^{Q^{\beta\beta}(2_1^+)+m_e c^2} d\epsilon_1 \times \int_{m_e c^2}^{Q^{\beta\beta}(2_1^+)+2m_e c^2-\epsilon_1} d\epsilon_2 \int_0^{Q^{\beta\beta}(2_1^+)+2m_e c^2-\epsilon_1-\epsilon_2} d\omega_1 \times f_{11}^{(0)} w_{2\nu} (\langle K_N \rangle - \langle L_N \rangle)^2 \quad (27)$$

where $Q(2_1^+) = Q^{\beta\beta} - E_x(2_1^+)$.
For the $0\nu\beta\beta$ decay and transitions to g.s. the PSF reads:

$$G_{0\nu}^{\beta\beta}(0^+ \to 0^+) = \frac{2}{4 g_A^4 R_A^2 \ln 2} \int_{m_e c^2}^{Q^{\beta\beta}+m_e c^2} f_{11}^{(0)} w_{0\nu} d\epsilon_1 \quad (28)$$

where

$$w_{0\nu} = \frac{g_A^4 (G\cos\theta_C)^4}{16\pi^5} (m_e c^2)^2 (\hbar c^2)(p_1 c)(p_2 c)\epsilon_1 \epsilon_2 \quad (29)$$

For transitions to the 2_1^+ states, one uses $Q(2_1^+)$ and instead of $f_{11}^{(0)}$ in Eq. (28), the next expression is integrated

$$f_{1+} + f_{1-} = 3(\frac{\hbar c}{m_e c^2 R_A})^2 (|f^{-2-1}|^2 + |f^{-1-2}|^2 + |f_{21}|^2 + |f_{12}|^2). \quad (30)$$

$$f^{-2-1} = g_{-2}(\epsilon_1) g_{-1}(\epsilon_2)\ ;\ f_{21} = f_2(\epsilon_1) f_1(\epsilon_2), \quad (31)$$

$$f^{-1-2} = g_{-1}(\epsilon_1) g_{-2}(\epsilon_2)\ ;\ f_{12} = f_1(\epsilon_1) f_2(\epsilon_2) \quad (32)$$

In our calculations, the Fermi constant is $G = 1.16637 \times 10^{-5}$ GeV^{-2} and $\cos\theta_C$=0.9737. In Eq.(23) it is convenient to redefine the PSF by a renormalization that eliminates the constant g_A and correlates (by dividing by $4R_A^2$) the dimension of $G_{0\nu}$ with the NME which are dimensionless. These are reflected in the lifetimes formulas (1). Thus, the PSF are also reported in $[yr^{-1}]$. A similar expression as equation (28) is employed in the PSF calculation for the transitions to excited 0_1^+ states, but replacing $Q^{\beta\beta}$ by $Q^{\beta\beta}(0_1^+)$. The formula used for the PSF computation for $2\nu\beta^+\beta^+$ decay mode is similar to that used for $2\nu\beta^-\beta^-$ decay, but $\epsilon_{1,2}$ are now the positron energies. Also, we use the same approximations as described above, to evaluate the radial positron w. f. (g and f) at the nuclear surface and replace the excitation energy E_N in the intermediate odd-odd nucleus by a suitable average energy.

2.3.2. The $EC\beta^+$ case

For the $EC\beta^+$ decays the energy released in the process is $Q^{EC\beta} = M(A, Z_0) - M(A, Z_0 - 2) - 2mc_e^2$. If the numerical solutions of the Dirac equation are obtained in Bohr units a_0, the probability that an electron is found on the surface of a nucleus of radius R_A can be defined as:

$$B_{n,\kappa}^2 = \frac{1}{4\pi(m_e c^2)^3}\left(\frac{\hbar c}{a_0}\right)^3\left(\frac{a_0}{R_A}\right)^2[g_{n,\kappa}^2(R_A) + f_{n,\kappa}^2(R_A)] \tag{33}$$

The PSF expression for $2\nu\beta\beta$ decay mode is

$$\begin{aligned} G_{2\nu}^{EC\beta^+} = {} & \frac{2A^2}{3\ln 2}\frac{(G\cos\theta)^4}{16\pi^5\hbar}(m_e c^2)\sum_{i=0,1}B_{i,-1}^2 \\ & \times\int_{m_e c^2}^{Q^{EC\beta}+\epsilon_{i,-1}+m_e c^2}\int_0^{Q^{EC\beta}+\epsilon_{i,-1}-\epsilon_p+m_e c^2} \\ & \times[g_{-1}^2(\epsilon_p) + f_1^2(\epsilon_p)] \\ & \times(\langle K_N\rangle^2 + \langle L_N\rangle^2 + \langle K_N\rangle\langle L_N\rangle)\omega_1^2\omega_2^2 p_p c\epsilon_p d\omega_1 d\epsilon_p \end{aligned} \tag{34}$$

where $\epsilon_{n,\kappa}$ are the binding energies of the electron while p_p and ϵ_p are the momentum and the energy of the positron. Here, the expressions for $\langle K_N\rangle$ and $\langle L_N\rangle$ are similar to those from Eqs. (24)-(25), but where ϵ_1 is replaced by $\epsilon_{i,-1}^c = m_e c^2 - \epsilon_{i,-1}$, the energy of the captured electron and ϵ_2 is replaced by ϵ_p, the energy of the emitted positron. For the $0\nu\beta\beta$ decay process the PSF expression is:

$$\begin{aligned} G_{0\nu}^{EC\beta^+} = {} & \frac{1}{4R_A^2}\frac{2}{\ln 2}\frac{(G\cos\theta)^4}{4\pi^3}(\hbar c^2)(m_e c^2)^5 \\ & \times\sum_{i=0,1}B_{i,-1}^2[g_{-1}^2(\epsilon_{p,i}) + f_1^2(\epsilon_{p,i})]p_p c\epsilon_p \end{aligned} \tag{35}$$

where $\epsilon_{p,i}$ denotes the maximal value of the positron associated to the state i.

2.3.3. The $2\nu ECEC$ case

The PSF expression is defined as:

$$\begin{aligned} G_{2\nu}^{ECEC} = {} & \frac{2\tilde{A}^2}{3\ln 2}\frac{(G\cos\theta)^4}{16\pi^3\hbar}(m_e c^2)^4 \times\sum_{i,j=0,1}B_{i,-1}^2 B_{j,-1}^2\int_0^{Q^{ECEC}+\epsilon_{i,-1}+\epsilon_{j,-1}} \\ & \times(\langle K_N\rangle^2 + \langle L_N\rangle^2 + \langle K_N\rangle\langle L_N\rangle)\omega_1^2\omega_2^2 d\omega_1 \end{aligned} \tag{36}$$

where $Q^{ECEC} = M(A, Z_0) - M(A, Z_0 - 2)$ is the energy released in the process. The expressions for $\langle K_N\rangle$ and $\langle L_N\rangle$ are similar to those from Eqs. (24)-(25), but where $\epsilon_{(1,2)}$ are replaced by $\epsilon_{(i,j)-1}^c = m_e c^2 - \epsilon_{(i,j)-1}$, the energies of the captured electrons.

Table 1

PSF for $\beta^-\beta^-$ decays to final g.s.

Nucleus	$Q^{\beta^-\beta^-}_{g.s.}$	$G^{\beta^-\beta^-}_{2\nu}$ (10^{-21} yr^{-1})				$G^{\beta^-\beta^-}_{0\nu}$ (10^{-15} yr^{-1})			
	(MeV)	This work	[5]	[28–30]	[32]	This work	[5]	[28–30]	[32]
^{48}Ca	4.267	15536	15550	16200	16200	24.65	24.81	26.1	26.0
^{76}Ge	2.039	46.47	48.17	53.8	52.6	2.372	2.363	2.62	2.55
^{82}Se	2.996	1573	1596	1830	1740	10.14	10.16	11.4	11.1
^{96}Zr	3.349	6744	6816		7280	20.48	20.58		23.1
^{100}Mo	3.034	3231	3308	3860	3600	15.84	15.92	18.7	45.6
^{110}Pd	2.017	132.5	137.7			4.915	4.815		
^{116}Cd	2.813	2688	2764		2990	16.62	16.70		18.9
^{128}Te	0.8665	0.2149	0.2688	0.35	0.344	0.5783	0.5878	0.748	0.671
^{130}Te	2.528	1442	1529	1970	1940	14.24	14.22	19.4	16.7
^{136}Xe	2.458	1332	1433	2030	1980	14.54	14.58	19.4	17.7
^{150}Nd	3.371	35397	36430	48700	48500	61.94	63.03	85.9	78.4
^{238}U	1.144	98.51	14.57			32.53	33.61		

3. NUMERICAL DETAILS

The numerical solutions of the Dirac equation were obtained by using the power series method of Ref. [36]. We built up a code that use a numerical algorithm similar to that described in Ref. [37], the normalization to unity for free states being done as indicated in Ref. [38].

In the numerical procedure, the potential energy as function of the distance r is approximated with a spline cubic function that interpolates values defined by an increment x. The radial w. f. is expanded as an infinite power series that depends on the increment and the coefficients of the spline function. Therefore, the values of the w. f. are calculated step by step in the mesh points. The accuracy of the solutions depends on the increment and the number of terms in the series expansion. We used an increment interval of 10^{-4} fm and at least 100 terms in the series expansion. These values exceed the convergence criteria of Ref. [37]. At very large distances, the behavior of the w. f. must resemble to that of the Coulomb function. This last condition provides a way to renormalize the amplitude to unity and to determine the phase shift. For discrete states, the asymptotic behavior of the w.f. gives a boundary for the inverse solutions. The eigenvalue is obtained when the direct solutions and the inverse ones match together.

In order to find the bound states of the electron, a procedure which differ from that given in Ref. [37] is developed. We start to compute numerical solution of the Dirac equation for a total energy close to $m_e c^2$, and we span an interval of 0.3 MeV under this energy in steps of 0.0002 MeV. In this range of energies, all the possible bound solutions are found. In the Ref. [37], the interval of the allowed solutions is

Table 2

PSF for $\beta^-\beta^-$ decays to final excited 0_1^+ states

Nucleus	$Q_{0_1^+}^{\beta^-\beta^-}$	$G_{2\nu}^{\beta^-\beta^-}(0_1^+)$ (10^{-21} yr^{-1})			$G_{0\nu}^{\beta^-\beta^-}(0_1^+)$ (10^{-15} yr^{-1})	
	(MeV)	This work	[5]	[32]	This work	[5]
^{48}Ca	1.270	0.3518	0.3627	0.376	0.3041	0.2989
^{76}Ge	0.9171	0.06129	0.06978	0.0769	0.1932	0.1776
^{82}Se	1.508	4.170		4.80	0.9440	
^{96}Zr	2.201	169.4	175.4	190	4.594	4.566
^{100}Mo	1.904	57.08	60.55	101	3.168	3.162
^{110}Pd	0.5472	3.3×10^{-3}	4.8×10^{-3}		0.1223	0.08844
^{116}Cd	1.056	0.7590	0.8737	0.89	0.7585	0.7163
^{130}Te	0.7335	0.05460	0.07566	18.6	0.3651	0.3086
^{136}Xe	0.8790	0.2823	0.3622	0.485	0.6746	0.6127
^{150}Nd	2.631	4116	4329	4850	26.96	27.27
^{238}U	0.2032	1.5×10^{-4}	4.6×10^{-4}		0.8229	0.7534

Table 3

PSF for $\beta^-\beta^-$ decays to final excited 2_1^+ states

Nucleus	$Q_{2_1^+}^{\beta^-\beta^-}$	$G_{2\nu}^{\beta^-\beta^-}(2_1^+)$ (10^{-21} yr^{-1})			$G_{0\nu}^{\beta^-\beta^-}(2_1^+)$ (10^{-15} yr^{-1})	
	(MeV)	This work	[27]	[32]	This work	[27]
^{48}Ca	3.284	4074	4410	4400	57.09	60.4
^{76}Ge	1.480	0.384	0.48	0.49	1.66	1.84
^{82}Se	2.219	69.6	90.6	85	12.13	13.8
^{96}Zr	2.571	745.5		850	33.87	
^{100}Mo	2.494	569.0		690	32.1	
^{110}Pd	1.359	0.46			2.41	
^{116}Cd	1.520	1.88		2.3	4.28	
^{128}Te	0.4255	6.8×10^{-7}	1.36×10^{-6}	1.3×10^{-6}	0.049	0.067
^{130}Te	1.990	79.6	116	120	18.34	22.8
^{136}Xe	1.640	7.68		15	8.31	
^{150}Nd	3.037	30308	45600	49000	223	301
^{238}U	1.099	2.66			26.3	

Table 4

PSF for $\beta^+\beta^+$ decay mode

Nucleus	$Q^{\beta^+\beta^+}$	$G_{2\nu}^{\beta^+\beta^+}$ (10^{-29} yr^{-1})			$G_{0\nu}^{\beta^+\beta^+}$ (10^{-20} yr^{-1})		
	(MeV)	This work	[6]	[29, 30]	This work	[6]	[29, 30]
^{78}Kr	0.8023	9159	9770	13600	243.2	250	293
^{96}Ru	0.6706	942.3	1040	1080	80.98	84.5	90.7
^{106}Cd	0.7314	1794	2000	1970	91.75	92.6	102
^{124}Xe	0.8203	4261	4850	4770	107.8	114	123
^{130}Ba	0.5748	91.54	110	47.9	23.82	25.7	21
^{136}Ce	0.3345	0.205	0.267	0.559	2.13	2.42	3.55

fixed by initial conditions, but its lower limit is an approximate one and sometimes the equations cannot be solved numerically.

For the PSF computation, all integrals are performed accurately with Gauss-Legendre quadrature in 32 points. We calculated up to 49 values of the radial functions in the Q value energy interval, that are interpolated with spline functions. In our calculations we used up-dated values of $Q^{\beta\beta}$ reported recently in Ref. [7].

4. RESULTS AND DISCUSSIONS

Our PSF values are presented in Tables 1-6, where, for comparison, other results from literature are also displayed. As we mentioned, the PSF values reported by KI in Refs. [5, 6] are obtained with a similar approach as ours, namely, the use of exact electron w.f. obtained by solving numerically the Dirac equation and with inclusion of the finite nuclear size and electron screening effects. The results reported in Refs. [27–29], [32] are obtained by approximating the electron w.f. at the nuclear surface and without inclusion of the screening effect.

The PSF values ($G_{2\nu}$, $G_{0\nu}$) for $\beta^-\beta^-$ decays are presented in Tables 1,2 and 3 for transitions to g.s and excited 0_1^+ and 2_1^+ states, respectively. For the transitions to g.s. (Table 1) our results are in very good agreement with the results reported in Ref. [5], the differences being under 5% for the large majority of cases, with two exceptions: the $G_{2\nu}$ values for the nuclei ^{128}Te (the difference is of 22%) and ^{238}U (the difference is of a factor 7; however, we think this large difference might be due to a possible uncontrolled numerical error in the value reported in [5]). For the transitions to excited 0_1^+ states (Table 2), there are several cases, especially for heavier nuclei (^{76}Ge, ^{110}Pd, ^{116}Cd, ^{130}Te, ^{136}Xe), where the differences between KI results and ours are in the range (10-40)%. Again, our $G_{2\nu}$ value for ^{238}U differs much from the KI result. The comparison between our results and those reported in

Refs. [27]-[28], [32] reveal larger discrepancies in several cases. For the transitions to excited 2_1^+ states (Table 3) there are no recent results reported, and the existent ones have been obtained with approximate w.f. Comparing our PSF values for 2_1^+ final states with those reported in Refs. [27], [32], one observes that the differences range in a 30% interval, both for $G_{0\nu}$ and $G_{2\nu}$. It is worth to mention that, although they are not yet measured, the $\beta^-\beta^-$ decays to excited 2_1^+ states are of interest to probe alternative mechanisms for occurrence of the 0ν-decay mode, to the (most common) mechanism of exchange of light LH neutrinos between two nucleons inside the nucleus.

The PSF values for the $\beta^+\beta^+$ decays are displayed in Table 4. One can see differences of (11-30)% between our $G_{2\nu}$ values and the KI ones, in majority of cases, while the agreement for $G_{0\nu}$ values is very good with one exception, for ^{136}Ce, where we got a difference of 13% compared with their value. The differences between our PSF values and those reported in [29] are larger in majority of results.

The results for $EC\beta^+$ decay mode are shown in Table 5 and they are grouped in two sectors: the first sector includes the six nuclei that can also undergo a $\beta^+\beta^+$ decay and the second one includes the other nuclei which can undergo only $EC\beta^+$ decays. One can see that the differences between KI results and ours are relevant in many cases. For the nuclei from the first sector (the most interesting experimentally cases, having the largest $Q^{EC\beta}$ values), we got several PSF values which differ by more than 20% compared to those reported by KI and other authors. For the "pure" $EC\beta^+$ decays, we got even more significant differences in several cases as compared with KI results, while other (older) results reported are a few.

Finally, the PSF values for the $2\nu ECEC$ decay mode are presented in Table 6. Here, the nuclei are grouped in three sectors: the first sector includes the six nuclei that can also undergo a $\beta^+\beta^+$ decay, the second one includes the nuclei that can also undergo $EC\beta^+$ decays and the third one includes the nuclei which can undergo only $2\nu ECEC$ decays. The differences between our $G_{2\nu}$ values and the KI ones for the nuclei from the first sector are within (30-55)%, while for the other nuclei they are even larger. The differences between the PSF values obtained with similar approaches (KI and ours) on the one side, and other previous results on the other side, might be explained by the use of less rigorous approaches, i.e. of approximate electron w.f, non-inclusion of the screening effect, (possible) less efficient routines at that time, etc. The differences between our results and those reported by KI may arise from the additional ingredients used in our approach, mentioned above. For example, we got relevant differences between their results and ours especially for decays where the $Q^{\beta\beta}$ values are small. In these cases the numerical precision in the integration of the PSF expressions is important and must be treated carefully. In these situations a large number of mesh points in the numerical integration over $Q^{\beta\beta}$ values is needed, in order to get stable results.

Table 5

PSF for $EC\beta^+$ decay mode

Nucleus	$Q^{EC\beta^+}$ (MeV)	$\epsilon_{0,-1}$ (keV)	$\epsilon_{1,-1}$ (keV)	$G_{2\nu}^{EC\beta^+}$ (10^{-24} yr^{-1})			$G_{0\nu}^{EC\beta^+}$ (10^{-18} yr^{-1})		
				This work	[6]	[29, 30]	This work	[6]	[29, 30]
^{78}Kr	1.824	17.7	3.1	338	385	464	6.90	6.34	7.11
^{96}Ru	1.693	26.2	4.9	372	407	454	11.30	9.62	10.8
^{106}Cd	1.753	31.1	5.9	741	702	779	15.39	13	14.7
^{124}Xe	1.842	39.4	7.8	1235	1530	1720	17.10	19.7	22.9
^{130}Ba	1.597	42.4	8.5	740	580	549	22.89	17.6	19.8
^{136}Ce	1.357	45.6	9.2	236	190	253	21.45	15.3	18.7
^{50}Cr	0.1469	8.3	1.2	1.62×10^{-6}	1.16×10^{-6}		0.376	0.0887	
^{58}Ni	0.9043	11.1	1.2	1.037	1.11	1.16	1.62	1.21	1.30
^{64}Zn	0.07269	12.6	2.0	2.21×10^{-8}	3.81×10^{-9}		0.546	0.0507	
^{74}Se	0.1872	16.0	2.7	2.2×10^{-5}	1.09×10^{-5}		0.9558	0.230	
^{84}Sr	0.7677	19.7	3.5	0.782	0.729		3.07	1.94	
^{92}Mo	0.6298	23.9	4.4	0.245	0.206		3.53	1.92	
^{102}Pd	0.1499	28.6	5.4	1.40×10^{-5}	1.62×10^{-6}		2.101	0.287	
^{112}Sn	0.8978	33.7	6.5	6.31	4.95		8.41	5.20	
^{120}Te	0.7082	36.5	7.1	1.406	0.730		7.61	3.92	
^{144}Sm	0.7604	52.3	10.7	3.56	2.49		10.38	8.11	
^{156}Dy	0.9840	59.6	12.4	48.1	25.3		26.01	15.2	
^{162}Er	0.8250	63.4	13.3	15.4	6.4	6.69	25.03	12.9	15.8
^{168}Yb	0.3873	67.4	14.0	9.1×10^{-3}	9.8×10^{-3}		16.48	4.23	
^{174}Hf	0.07689	71.6	15.2	7.5×10^{-6}	1×10^{-9}		10.81	0.0272	
^{184}Os	0.4289	80.4	17.3	0.321	0.0299		26.21	7.04	
^{190}Pt	0.3625	85.2	18.2	0.127	0.00588		27.61	5.57	

Our calculations are done with up to 49 interpolation points. Around the zero kinetic energy of the released electron/positron, we used an interval energy of about 10^{-4} MeV, because in this region a sudden variation of the w.f. amplitude is produced. We observed that after 40 interpolation points, the results remain unchanged, in all the cases. It is worth to mention that, in many cases, the use of a smaller number of mesh points can leads to results that can differ up to 20%. The use of a realistic Coulomb potential can also lead to differences of a few percent, especially for electron(s) captured decays. The use of recently reported $Q^{\beta\beta}$ values may also contribute to these differences. We first computed the PSF using both the same $Q^{\beta\beta}$ values used by KI and then with those taken from Ref. [7], and got differences up to 3% for several nuclei. In the cases involving bound electron states, important is the numerical accuracy in the identification of electron/positron bound state $1s_{1/2}$ that intervene in the Eq. (33). That is why we built up a different procedure for getting the correct electron/positron bound states, as it was described in Section 2. We tested the procedure described in Ref. [37] to obtain the bound states and we observed that the Eq. (59) of this reference can give two solutions. One of them is correct, giving the same number of nodes for the radial functions $f_{n,\kappa}$ and $g_{n,\kappa}$, while the other solution is useless because the number of nodes for the two amplitudes differs by one unity. The incorrect identification of the electron/positron bound state $1s_{1/2}$ can lead to significant differences between the obtained PSF values. These possible sources of uncertainties mentioned above can act cumulatively or not. In our opinion, differences larger that 10% between the values of different PSF computations are important for precise DBD calculations/estimations, hence the evaluation of the PSF for DBD is still a challenge.

5. CONCLUSIONS

We calculated the PSF involved in the $\beta^-\beta^-$, $\beta^+\beta^+$, $EC\beta^+$ and $2\nu ECEC$ DBD modes using exact electron w.f. obtained by solving numerically the Dirac equation and with inclusion of finite nuclear size and electron screening effects. In comparison with a recent similar approach described in Refs. [5, 6], our method of calculation includes several ingredients: i) the use a Coulomb potential derived from a realistic proton density distribution in nucleus; ii) new numerical routines both for solving the Dirac equations and integrating the PSF expressions; iii) a procedure to identify unambiguously the electron/positron bound states; iv) the use of $Q^{\beta\beta}$ values taken from a recent mass evaluation [7]. Also, we reported for the first time PSF values for transitions to final excited 2_1^+ states, computed with exact Dirac electron w.f. For each decay mode we got several relevant differences between our results and other similar ones, reported in literature. These ingredients, which can

Table 6

PSF for $2\nu ECEC$ decay mode

Nucleus	Q^{ECEC}	$\epsilon_{0,-1}$	$\epsilon_{1,-1}$	$G_{2\nu}^{ECEC}$ (10^{-24} yr^{-1})		
	(MeV)	(keV)	(keV)	This work	[6]	[29, 30]
^{78}Kr	2.846	17.7	3.1	410	660	774
^{96}Ru	2.715	26.2	4.9	1450	2400	2740
^{106}Cd	2.775	31.1	5.9	4299	5410	6220
^{124}Xe	2.864	39.4	7.8	15096	17200	20200
^{130}Ba	2.619	42.4	8.5	14773	15000	16300
^{136}Ce	2.379	45.6	9.2	12223	12500	15800
^{50}Cr	1.169	8.3	1.2	0.238	0.422	
^{58}Ni	1.926	11.1	1.2	9.90	15.3	17
^{64}Zn	1.095	12.6	2.0	1.03	1.41	
^{74}Se	1.209	16.0	2.7	3.41	5.65	
^{84}Sr	1.790	19.7	3.5	64.62	93.6	
^{92}Mo	1.652	23.9	4.4	82.32	208	
^{102}Pd	1.172	28.6	5.4	42.09	46	
^{112}Sn	1.920	33.7	6.5	869.7	1150	
^{120}Te	1.730	36.5	7.1	840.3	888	
^{144}Sm	1.782	52.3	10.7	6436	5150	
^{156}Dy	2.006	59.6	12.4	22078	17600	
^{162}Er	1.847	63.4	13.3	20085	15000	18100
^{168}Yb	1.409	67.4	14.0	7872	4710	
^{174}Hf	1.099	71.6	15.2	3432	1580	
^{184}Os	1.451	80.4	17.3	24222	12900	
^{190}Pt	1.384	85.2	18.2	28153	12900	
^{36}Ar	0.4326	5.0	1.2	2.9×10^{-4}		
^{40}Ca	0.1935	5.9	1.2	1.02×10^{-5}	1.25×10^{-5}	
^{54}Fe	0.6798	9.7	1.4	0.03021	0.0469	
^{108}Cd	0.2718	31.1	5.9	0.0682	0.0207	
^{126}Xe	0.9195	39.4	7.8	60.59	46.1	
^{132}Ba	0.8439	42.3	7.7	61.98	39.1	
^{138}Ce	0.6930	45.6	9.2	34.47	18.4	
^{152}Gd	0.05570	55.9	11.6	1.12×10^{-2}		
^{158}Dy	0.2829	59.6	12.4	3.191	0.183	
^{164}Er	0.02506	63.4	13.3	8.3×10^{-3}		
^{180}W	0.1433	75.8	16.0	1.4781	0.00156	
^{196}Hg	0.8206	89.9	19.5	3587	821	

act cumulatively or not, can be at the origin of these differences, and justify, in our opinion, a re-computation of the PSF with improved methods. Accurate values of the PSF (besides the NME) are very required in the DBD study, both for theorists to improve the lifetimes predictions and constraint the neutrino parameters [39], and for experimentalists [40], to plan their set-ups.

Acknowledgements. This work was supported by a grant of the Romanian Ministry of National Education, CNCS UEFISCDI, project PCE-2011-3-0318, Contract no. 58/28.10/2011.

REFERENCES

1. F. T. Avignone, S.R. Elliott, and J. Engel, Rev. Mod. Phys. **80**, 481 2008.
2. H. Ejiri, Prog. Part. Nucl. Phys., **4**, 249 (2010).
3. W. Rodejohann, Int. J. Mod. Phys. E **20**, 1833 (2011).
4. Vergados J, Ejiri H, and Simkovic F, Rep. Prog. Phys. **75**, 106301 (2012).
5. J. Kotila and F. Iachello, Phys. Rev. C **85**, 034316 (2012).
6. J. Kotila and F. Iachello, Phys. Rev. C **87**, 024313 (2013).
7. M. Wang, G. Audi, A.H. Wapstra, F.G. Kondev, M. MacCornick, X. Xu, and B. Pfeiffer, Chin. Phys. C **36**, 1603 (2012).
8. V.A. Rodin, A. Faessler, F. Simkovic, and P. Vogel, Phys. Rev. C **68**, 044302 (2003).
9. F. Simkovic, A. Faessler, V.A. Rodin, P. Vogel, and J. Engel, Phys. Rev. C **77**, 045503 (2008).
10. F. Simkovic, A. Faessler, H. Muther, V. Rodin, and M. Stauf, Phys. Rev. C **79**, 055501 (2009).
11. Dong-Liang Fang, Amand Faessler, Vadim Rodin, Fedor Simkovic, Phys. Rev. C 83, 034320 (2011).
12. M. Kortelainen, O. Civitarese, J. Suhonen, and J. Toivanen, Phys. Lett. B **647**, 128 (2007).
13. M. Kortelainen and J. Suhonen, Phys. Rev. C **75**, 051303(R) (2007).
14. S. Stoica and H.V. Klapdor-Kleingrothaus, Nucl. Phys. A**694**, 269 (2001).
15. E. Caurier, A.P. Zuker, A. Poves, and G. Martinez-Pinedo, Phys. Rev. C **50**, 225 (1994); J. Retamosa, E. Caurier and F. Nowacki, Phys. Rev. C **51**, 371 (1995).
16. E. Caurier, J. Menendez, F. Nowacki, and A. Poves, Phys. Rev. Lett. **100**, 052503 (2008).
17. J. Menendez, A. Poves, E. Caurier, F. Nowacki, and A. Poves, Nuclear Physics A **818**, 139 (2009).
18. M. Horoi, S. Stoica, and B.A. Brown, Phys. Rev. C **75**, 034303 (2007).
19. M. Horoi and S. Stoica, Phys. Rev. C **81**, 024321 (2010).
20. J. Barea and F. Iachello, Phys. Rev. C **79**, 044301 (2009).
21. J. Barea, J. Kotila, and F. Iachello, Phys. Rev. Lett. **109**, 042501 (2012).
22. T.R. Rodriguez and G. Martinez-Pinedo, Phys. Rev. Lett **105**, 252503 (2010).
23. A. Neacsu and S. Stoica, Rom. Rep. Phys. **66**, 376 (2014).
24. P.K. Rath, R. Chandra, K. Chaturvedi, P.K. Raina, and J.G. Hirsch, Phys. Rev. C **82**, 064310 (2010).
25. H. Primakov and S.P. Rosen, Rep. Prog. Phys. **22**, 121 (1959).
26. W.C. Haxton and G.J. Stephenson Jr., Prog. Theor. Part. Nucl. Phys. **12**, 409 (1984).
27. M. Doi, T. Kotani, H. Nishiura, and E. Takasugi, Prog. Theor. Phys. **69**, 602 (1983).
28. M. Doi, T. Kotani and E. Takasugi, Prog. Theor. Phys. Suppl. **83**, 1 (1985).
29. M. Doi and T. Kotani, Prog. Theor. Phys. **87**, 1207 (1992).

30. M. Doi and T. Kotani, Prog. Theor. Phys. **89**, 139 (1993).
31. T. Tomoda, Rep. Prog. Phys. **54**, 53 (1991).
32. J. Suhonen and O. Civitarese, Phys. Rep. **300**, 123 (1998).
33. S. Esposito, Am. J. Phys. **70**, 852 (2002).
34. S. Stoica and M. Mirea, Phys. Rev. C **88**, 037303 (2013).
35. T.E. Pahomi, A. Neacsu, M. Mirea, and S. Stoica, Rom. Rep. Phys. **66**, 370 (2014).
36. W. Buhring, Z. Phys. **187**, 180 (1965).
37. F. Salvat, and R. Mayol, Comp. Phys. Commun. **62**, 65 (1991)
38. F. Salvat, J.M. Fernandez-Varea, and W. Williamson Jr, Comp. Phys. Commun. **90**, 151 (1995).
39. A.S. Barabash, Nucl. Phys. A **935**, 52 (2015).
40. R. Arnold, et al., Phys. Rev. D **89**, 111101 (2014).